Honeycomb lattice Na_2IrO_3 at high pressures: A robust spin-orbit Mott insulator

Xiaoxiang Xi,[1,2,3,*] Xiangyan Bo,[1,2] X. S. Xu,[4] P. P. Kong,[5] Z. Liu,[6] X. G. Hong,[7,8] C. Q. Jin,[5] G. Cao,[9] Xiangang Wan,[1,2,†] and G. L. Carr[3]

[1]*National Laboratory of Solid State Microstructures and Department of Physics, Nanjing University, Nanjing 210093, China*
[2]*Collaborative Innovation Center of Advanced Microstructures, Nanjing University, Nanjing 210093, China*
[3]*Photon Sciences, Brookhaven National Laboratory, Upton, New York 11973, USA*
[4]*Department of Physics and Astronomy, University of Nebraska, Lincoln, Nebraska 68588, USA*
[5]*Institute of Physics, Chinese Academy of Sciences, Beijing 100190, China*
[6]*Institute of Materials Science and Department of Civil and Environmental Engineering, The George Washington University, Washington D.C. 20052, USA*
[7]*Mineral Physics Institute, Stony Brook University, Stony Brook, New York 11794, USA*
[8]*Center for High Pressure Science and Technology Advanced Research, Beijing 100094, China*
[9]*Department of Physics, University of Colorado at Boulder, Boulder, Colorado 80309, USA*

(Received 7 January 2018; revised manuscript received 12 April 2018; published 10 September 2018)

The honeycomb iridate Na_2IrO_3 has received much attention as a candidate to realize a quantum spin liquid state, but the nature of its insulating state remains controversial. We found that the material exhibits structural transitions at 3 and 10 GPa. The former is accompanied by 166-meV suppression of the activation gap, but the energies for the low-lying interband transitions change by less than 10 meV. This can be reconciled in a picture in which the application of high pressure barely shifts the electronic bands, but rather merely broadens them. First-principles calculations uncover a strong correlation between the band gap and the β angle of the monoclinic structure, indicating non-negligible interlayer coupling. These results offer clear evidence for a spin-orbit Mott insulating state in Na_2IrO_3 and are inconsistent with the quasimolecular orbital model.

DOI: 10.1103/PhysRevB.98.125117

The insulating state in iridium oxides came as a surprise. With greater spatial extent of the 5*d* electron orbitals than in 3*d* transition metal oxides, the iridates were speculated to have large bandwidth W and small Coulomb interaction U, disobeying the $U > W$ Mott criterion [1]. The importance of spin-orbit coupling (SOC) in this class of materials was only recognized in the past decade, culminating in the notion of spin-orbit-assisted Mott insulators [2–5]: SOC (with strength λ) splits the Ir t_{2g} orbitals near the Fermi level and entangles them with spin to form bands with effective angular momenta $J_{\text{eff}} = 1/2$ and $3/2$; exchange splitting under a small U then opens a Mott gap E_g in the narrow $J_{\text{eff}} = 1/2$ band [Fig. 1(a)]. The interplay of SOC and electron correlation is expected to generate exotic ground states [6–11], including the quantum spin Hall effect [12], quantum spin liquid [13,14], and a topological insulating phase [15,16]. While Sr_2IrO_4 is now generally accepted as a spin-orbit Mott insulator [2–4], the nature of the ground state of other iridates such as Na_2IrO_3 is yet to be clarified.

Na_2IrO_3 has received much attention due to the possibility of a novel quantum spin liquid state [13,14,17–34], described in the Kitaev model [35], but the nature of its insulating state remains controversial. Because a gap of ~340 meV [36] is already open far above the zigzag antiferromagnetic [18,21,23] ordering temperature, the Slater-type mechanism was ruled out. As a close cousin of Sr_2IrO_4, initially Na_2IrO_3 was also considered a spin-orbit Mott insulator. Early angle-resolved photoemission spectroscopy [36], optics [36], and resonant inelastic x-ray scattering [37] data were interpreted in this picture. Noting that Na_2IrO_3 has edge-sharing IrO_6 octahedra forming a honeycomb lattice [Fig. 1(b)] and the nearest-neighbor oxygen-assisted hopping is highly anisotropic, Mazin *et al.* proposed that the electron hopping is mainly confined within one honeycomb, forming nearly dispersionless quasimolecular orbitals (QMOs) [38,39]. New optics data were thought to support this model [40,41]. These two scenarios appear contradictory, featuring localized and itinerant electronic states, respectively. However, they were recently unified in a theoretical framework, demonstrating a crossover between the two tuned by either SOC or U [42]. Based on the magnitude of λ and U in Na_2IrO_3, it was argued that a spin-orbit Mott insulator should be stabilized [42], which still awaits experimental confirmation. Establishing Na_2IrO_3 as a spin-orbit Mott insulator is a prerequisite for realizing the Kitaev quantum spin liquid state in this material.

In this paper, we investigate the insulating state in Na_2IrO_3 using a combination of high-pressure experiments and first-principles calculations. The in-plane resistance drops precipitously by more than one order of magnitude across a structural transition near 3 GPa [43], while the energies of the low-lying interband transitions do not experience a significant change. This can be well accounted for by the spin-orbit Mott insulating state, in which the application of high pressure

*Corresponding author: xxi@nju.edu.cn
†Corresponding author: ccmp@nju.edu.cn

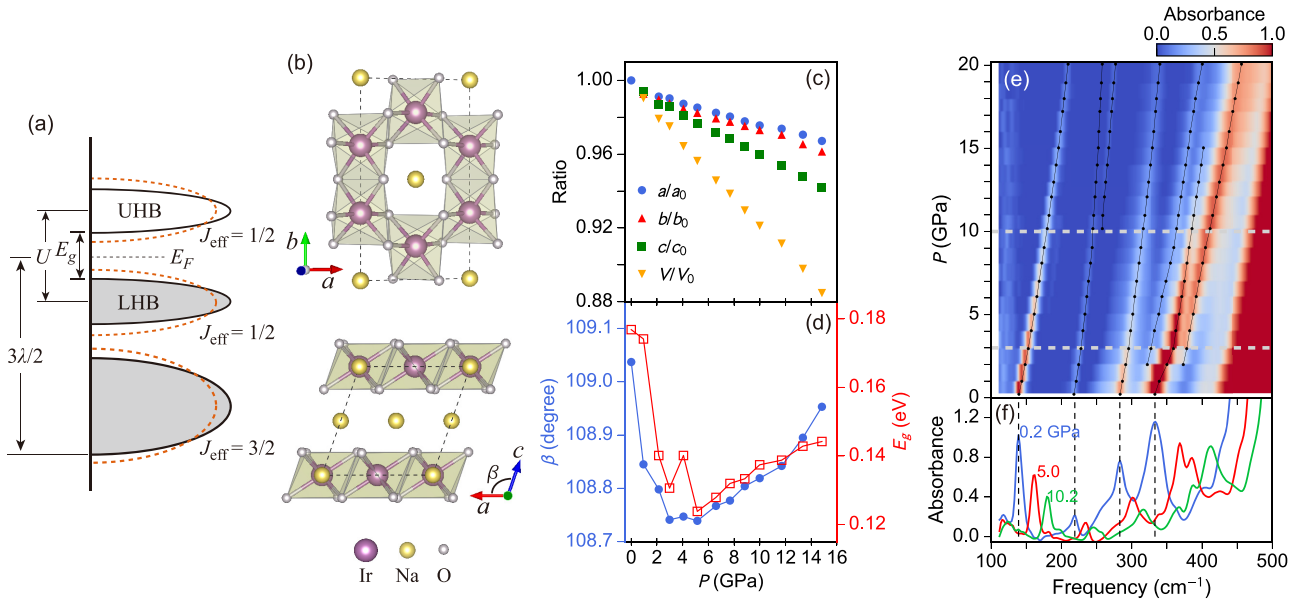

FIG. 1. (a) Schematic for the formation of a spin-orbit Mott insulator. The $J_{\rm eff} = 1/2$ and $3/2$ bands form due to SOC with strength λ. Coulomb repulsion U splits the $J_{\rm eff} = 1/2$ band into an upper Hubbard band (UHB) and a lower Hubbard band (LHB), resulting in a band gap E_g at the Fermi level E_F. The dotted lines depict bandwidth broadening. (b) Crystal structure of Na_2IrO_3 [46]. (c) Pressure dependence of the unit-cell dimensions and volume, normalized to their respective ambient-pressure values from Ref [21]. (d) Pressure dependence of the β angle (left scale) and E_g from first-principles calculations (right scale). (e) Far-infrared absorbance contour as a function of the photon frequency and pressure, with representative spectra at 0.2, 5.0, and 10.2 GPa shown in (f). The dots in (e) are peak frequencies determined by fitting analysis [47]. The horizontal dashed lines delineate pressures for structural transitions.

barely shifts the energy bands (because they are mainly determined by the pressure-independent SOC and U) but merely broadens them, diminishing the activation gap and rendering the material less insulating [see an illustration in Fig. 1(a)]. Calculations further reveal that the band gap is sensitively controlled by the β angle that dictates the interlayer stacking offset, suggesting a route for bandwidth control via interlayer hybridization. Our comprehensive study provides a coherent picture for Na_2IrO_3 as a robust spin-orbit Mott insulator, paving the way for exploring novel physics in this intriguing material.

Na_2IrO_3 single crystals were synthesized from off-stoichiometric quantities of IrO_2 and Na_2CO_3 using a self-flux method [23]. Freshly cleaved platelets were used in the infrared spectroscopy and resistance measurements, while fine powder ground from the crystals was used in x-ray powder diffraction (XRD). All high-pressure experiments employed the diamond-anvil cell technique. Infrared spectroscopy and XRD were performed at Beamlines U2A and X17C, respectively, of the National Synchrotron Light Source, Brookhaven National Laboratory (see details in Ref. [44]). Four-probe resistance measurements were performed using a CuBe cell with Au electrodes, as described elsewhere [45].

We first investigated the stability of the crystal structure under pressure. Na_2IrO_3 is a layered material with the monoclinic space group $C2/m$ [21,23]. In the ab plane, edge-sharing IrO_6 octahedra form a honeycomb lattice. The layers stack along the c axis with $\beta = 109.037^\circ$ and are separated by sodium atoms [Fig. 1(b)]. XRD data up to 14.8 GPa can be fit well based on this known crystal structure [47], yielding the pressure dependence of the lattice parameters shown in Figs. 1(c) and 1(d). A smooth contraction is seen along all three axes. Interestingly, the β angle goes through a minimum near 4 GPa, where it decreases slightly by 0.3° from the ambient-pressure value. This is in contrast to the monotonic increases up to 25 GPa reported in Ref. [48], calling for further investigations to resolve the discrepancy.

The structural anomaly signified by the β angle is further corroborated by infrared spectroscopy of phonons. Figure 1(f) shows the near-ambient absorbance as the blue line, acquired by polarizing the electric field in the ab plane. Four phonon modes are clearly identified at 139, 219, 283, and 333 cm^{-1}. Modes above 400 cm^{-1} absorb light more strongly and saturate the absorbance [47]. Upon increasing pressure, the 333 cm^{-1} mode evolves into three, with itself exhibiting a kink in the pressure dependence of the frequency at 3 GPa [see Fig. 1(e) and [47]]. At 10 GPa, the 219 cm^{-1} mode splits into two. Combined with anomalous pressure dependence in the linewidth and oscillator strength of these phonon modes [47], we deduce pressure-induced structural transitions near 3 and 10 GPa. The smooth compression of the unit-cell volume [Fig. 1(c)] suggests second-order nature of these transitions. The phonon data shown here set constraints on possible structures at high pressure predicted by theory [49].

We next focus on pressure effects on the electronic structure. In Na_2IrO_3, the low-lying interband transitions fall in the midinfrared, with typical absorbance spectra shown in Fig. 2(a). Apart from a pronounced phonon mode below 0.1 eV, the absorbance is dominated by two broad peaks with significant overlap. These peaks were also seen in Ref. [40], but overlooked in Refs. [36,48]. They can be understood as due to the interband transitions from the two valence bands

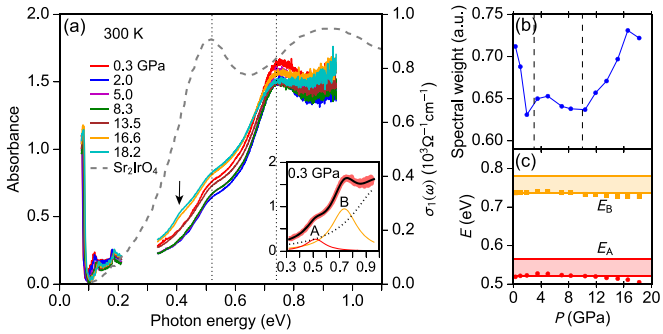

FIG. 2. (a) Midinfrared absorbance of Na_2IrO_3 under pressure (left scale). The inset shows a fit of the data at 0.3 GPa. The ambient-pressure optical conductivity of Sr_2IrO_4 (thick dashed line) from Ref. [56] is shown for comparison (right scale). (b) Pressure dependence of the spectral weight of the absorbance between 0.34 and 0.94 eV. The dashed lines indicate the pressures for the structural transitions found in Fig. 1(e). (c) Pressure dependence of the peak energies E_A and E_B obtained by fitting analysis of the absorbance. The shaded regions represent the expected amount of pressure-induced increase in the QMO picture.

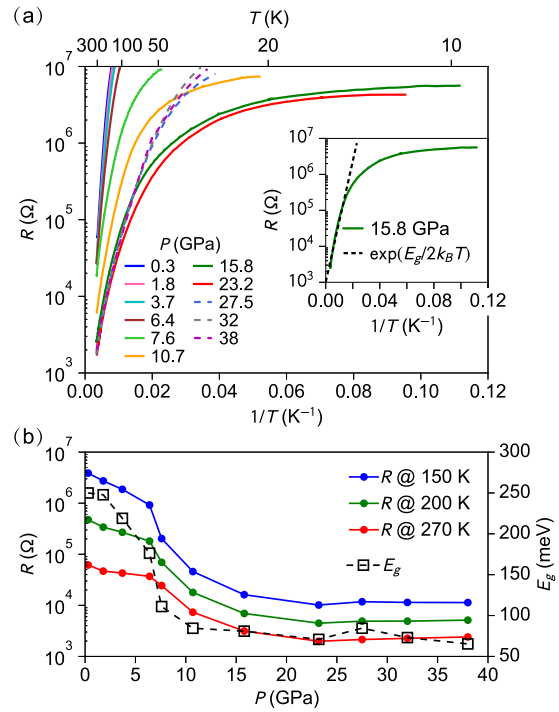

FIG. 3. (a) Temperature dependence of the in-plane resistance of Na_2IrO_3 under pressure. The lower scale is in $1/T$ and the upper scale in T. The inset shows a fit of the data at 15.8 GPa in the high-temperature region to the form $e^{E_g/2k_BT}$. (b) Pressure dependence of the resistance at selected temperatures (left scale). The open squares are the fitted activation gap (right scale).

closest to the Fermi level to the lowest-lying conduction band, regardless of the physical origin of these bands [47]. Under pressure, the overall spectral weight experiences a nonmonotonic change [47]. Figure 2(b) shows the integrated area under absorbance from 0.34 to 0.94 eV as a function of pressure. Kinks are observed near 3 and 10 GPa, consistent with the pressures for the structural transitions. A small hump at ~0.4 eV gradually develops above 10 GPa [highlighted by the arrow in Fig. 2(a)], possibly due to changes of the electronic structure associated with the second structural transition.

Figure 2(a) (inset) shows a fit of the absorbance at 0.3 GPa. A summation of two Lorentzian functions with a third Lorentzian background (to account for higher-energy transitions [40]) fits the data well, yielding $E_A = 0.52$ eV and $E_B = 0.74$ eV. Because the background has significant spectral weight and peaks A and B overlap strongly, to reliably disentangle the individual spectral weight for each peak is difficult. We instead focus on the peak energies, which are already clearly identified in the raw spectra. Upon increasing pressure up to 18.2 GPa, peaks A and B shift marginally, indicated by the vertical dotted lines in Fig. 2(a). Fitting analysis shows that E_A and E_B experience a minor change of 22 and 10 meV, respectively, up to 18.2 GPa [Fig. 2(c)]. Note that the phonon mode near 0.1 eV, the strong absorption between 0.21 and 0.33 eV by the diamond-anvil cell, and the thermal broadening conspire to obscure the absorption onset, which should otherwise serve to quantify the band gap.

We resort to electrical transport to gain information about the band gap. Figure 3(a) shows the temperature dependence of the in-plane resistance. At differing pressures up to 38 GPa the resistance increases rapidly upon cooling, suggesting that the insulating state is robust under pressure. Between 10.7 and 23.2 GPa the resistance can be measured over an extended temperature range, showing saturation below 20 K, a signature of conduction via impurity states [47,50]. We focus on the high-temperature end (above 150 K) where data at different pressures can all be fit to the form $e^{E_g/2k_BT}$, where k_B is the Boltzmann constant. An example fit at 15.8 GPa is shown in Fig. 3(a) (inset). The pressure dependence of E_g is shown as open squares in Fig. 3(b). At ambient pressure, $E_g \simeq 250$ meV. Increasing pressure induces a drastic decline of E_g starting at 4 GPa, nearly coinciding with that for the first structural transition. Above 16 GPa, E_g levels off to approximately 70 meV. We extract the resistance at different pressures for selected temperature points above 100 K. Figure 3(b) shows that its pressure dependence is similar to that of E_g, confirming that the electrical transport above 150 K is dominated by thermally activated conduction.

Remarkably, the activation gap diminishes by $\Delta E_g = 166$ meV up to near 10 GPa, while the low-lying interband transition energies change by less than 10 meV in the same pressure range. This implies that the application of high pressure barely shifts the electronic bands but broadens them due to enhanced electron hopping, resulting in reduced E_g. These results hold important clues about whether the spin-orbit Mott insulator or the QMO picture fits Na_2IrO_3.

In the former picture, peak A (B) is assigned as due to the optical transition from the lower Hubbard band ($J_{\rm eff} = 3/2$ band) to the upper Hubbard band, hence $E_A = U$ and $E_B = (U + 3\lambda)/2$ [see Fig. 1(a)]. Since both U and λ are dominated by iridium atomic properties and therefore insensitive to pressure, both E_A and E_B are expected to be stable under pressure. This is highly consistent with our data shown in Fig. 2, offering clear evidence for a spin-orbit Mott insulating state in Na_2IrO_3. Quantitatively, we estimate $U = E_A = 0.52$ eV and

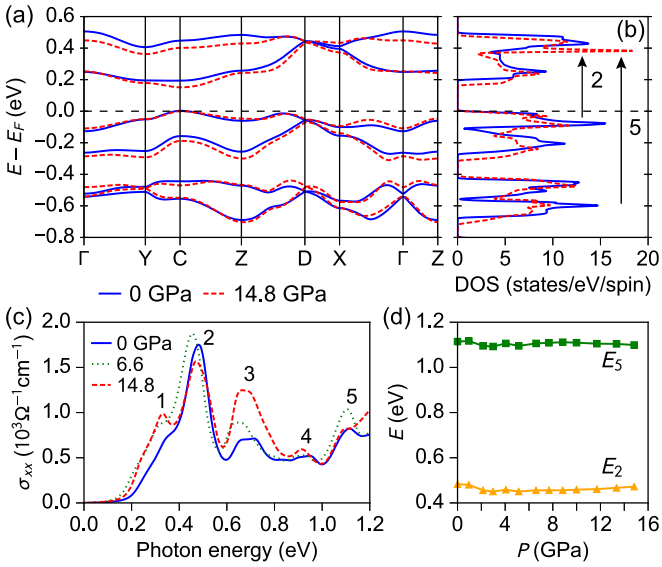

FIG. 4. LSDA + U + SOC calculation results for Na_2IrO_3: (a) electronic band structure, (b) density of states, and (c) in-plane optical conductivity. (d) Pressure dependence of the peak energies in the optical conductivity that correspond to the transitions 2 and 5.

$\lambda = (2E_B - E_A)/3 = 0.32$ eV, consistent with the expected values for $5d$ electrons, $U \sim 0.4$–2 eV and $\lambda \sim 0.1$–1 eV [11].

In the QMO model, considering only the oxygen-assisted nearest-neighbor hopping t, an A_{1g} singlet and an E_{2u} doublet constitute the lowest-lying bands near the Fermi level, with eigenenergies of $2t$ and t, respectively [38]. Inclusion of SOC splits the E_{2u} doublet [42]. Peaks A and B are therefore assigned as due to the optical transitions from the split E_{2u} to the A_{1g} QMOs. In the limit of small SOC, as assumed by the QMO model, the transition energies are $E_A = t - \lambda/2$ and $E_B = t + \lambda/2$. Since t is determined by the orbital overlap and hence the unit-cell volume, it is expected that pressure-induced volume contraction should shift both peaks to higher energies, with an amount denoted as Δt. One can estimate Δt by noting $W \sim 4t$ [51] and $\Delta W \sim \Delta E_g$, yielding $\Delta t \sim$ 42 meV, well within our spectral resolution. This amount of shift for peaks A and B is shown as shaded regions in Fig. 2(c), in stark contrast to the small changes observed in our experiment.

To further gain insight into the effects of pressure on the electronic structure, we performed local spin density approximation (LSDA) + U calculations including SOC, using the pressure-dependent lattice parameters. The methods are described in [47]. The structural transitions were neglected because of the lack of high-pressure structural details. Due to the antiferromagnetic order inherent in the theoretical model, the number of bands doubles. The optical conductivity therefore exhibits more interband transition peaks than observed experimentally. Figure 4(c) shows the dominant in-plane component of the optical conductivity tensor σ_{xx} at selected pressures. We track the pressure evolution of two peaks, i.e., 2 and 5, each associated with one group of bands just below the Fermi level. The maximum change of the peak energy is 33 and 24 meV, respectively [Fig. 4(d)], slightly higher than the amount obtained experimentally. This suggests that the band energies are robust even in the presence of structural transitions, supporting the spin-orbit Mott insulator scenario.

Our calculations further reveal a striking correlation between the band gap and the β angle under pressure, albeit the subtle change for the latter [Fig. 1(d)]. Increasing β from 90° results in enhanced offset of the atomic positions between the IrO_6 honeycomb layers [see Fig. 1(b)]. Interlayer hybridization via oxygen and sodium orbitals is suppressed accordingly, leading to bandwidth reduction and band gap increase. Tuning β away from 90° therefore effectively drives the system from three-dimensional-like toward two-dimensional, reminiscent of the dimensionality-controlled insulator-metal transition in $Sr_{n+1}Ir_nO_{3n+1}$ [3]. Although the correlation between the band gap and β was not observed experimentally due to the complications from structural transitions, it implies the importance of interlayer coupling in Na_2IrO_3, inconsistent with the QMO model that assumes purely intralayer electron hopping.

We lastly discuss the role of trigonal distortion. The J_{eff} description for the spin-orbit Mott insulators assumes regular IrO_6 octahedra, but structural studies found trigonal distortion in Na_2IrO_3 [21,23], whose role was emphasized by some authors [15,40,52] but considered minimal by others [37,38]. Large trigonal distortion has been shown to mix the $J_{\text{eff}} = 1/2$ and $J_{\text{eff}} = 3/2$ states, invalidating the J_{eff} description [53]. The degree of trigonal distortion is generally altered under high pressure, exemplified by the pyrochlore $Cd_2Re_2O_7$ [54] and $Eu_2Sn_2O_7$ [55]. Therefore, if the trigonal distortion is crucial for forming the low-lying bands in Na_2IrO_3, the interband transitions are expected to change under pressure. This is inconsistent with our result. We also note that both Sr_2IrO_4 and Na_2IrO_3 show double peaks in their optical absorption below 1 eV [see Fig. 2(a)]. Their lower-energy peaks coincide remarkably in energy, suggesting that the J_{eff} description applies for both materials, with the same magnitude of U determined by the iridium atoms. The higher-energy peaks appear at different energies, possibly due to the material-specific trigonal distortion that perturbs the J_{eff} bands differently.

In summary, we found pressure-induced structural transitions in Na_2IrO_3 at 3 and 10 GPa. The lowest-lying interband transition energies are stable across 3 GPa, offering clear evidence for a spin-orbit Mott insulating state. Above 10 GPa, another interband transition peak develops at low energy, signifying the breakdown of the J_{eff} description. Dimerization transitions were recently found in layered honeycomb magnets α-Li_2IrO_3 [57,58] and α-$RuCl_3$ [59,60] at 3.8 and 0.8 GPa, respectively. Unlike these materials, our results suggest Na_2IrO_3 as a robust spin-orbit Mott insulator up to at least 10 GPa, motivating further exploring the interplay of electron correlation and SOC, especially for realizing the Kitaev spin liquid by lattice modulation [20,28,29].

We are grateful for helpful discussions with W. Ku and R. Valentí. This work was supported by National Key R&D Program of China (Grants No. 2018YFA0307000 and No. 2017YFA0303201), the Fundamental Research Funds for the Central Universities (0204-14380047), and the U.S. Department of Energy through Contract No. DE-AC02-98CH10886 at BNL. The use of U2A and X17C beamlines was supported by NSF (DMR-0805056; EAR 06-49658, COMPRES) and

DOE/NNSA (DE-FC03-03N00144, CDAC). X.-G.W. was supported by the NSFC (Grant No. 11525417). G.C. acknowledges support by the U.S. National Science Foundation via Grant No. DMR-171210.

[1] G. Cao and L. De-Long, *Frontiers of 4d- and 5d-Transition Metal Oxides* (World Scientific, Singapore, 2013).
[2] B. J. Kim, H. Jin, S. J. Moon, J.-Y. Kim, B.-G. Park, C. S. Leem, J. Yu, T. W. Noh, C. Kim, S.-J. Oh, J.-H. Park, V. Durairaj, G. Cao, and E. Rotenberg, Phys. Rev. Lett. **101**, 076402 (2008).
[3] S. J. Moon, H. Jin, K. W. Kim, W. S. Choi, Y. S. Lee, J. Yu, G. Cao, A. Sumi, H. Funakubo, C. Bernhard, and T. W. Noh, Phys. Rev. Lett. **101**, 226402 (2008).
[4] B. J. Kim, H. Ohsumi, T. Komesu, S. Sakai, T. Morita, H. Takagi, and T. Arima, Science **323**, 1329 (2009).
[5] H. Watanabe, T. Shirakawa, and S. Yunoki, Phys. Rev. Lett. **105**, 216410 (2010).
[6] D. Pesin and L. Balents, Nat. Phys. **6**, 376 (2010).
[7] X. Wan, A. M. Turner, A. Vishwanath, and S. Y. Savrasov, Phys. Rev. B **83**, 205101 (2011).
[8] W. Witczak-Krempa, G. Chen, Y. B. Kim, and L. Balents, Annu. Rev. Condens. Matter Phys. **5**, 57 (2014).
[9] J. G. Rau, E. K.-H. Lee, and H.-Y. Kee, Annu. Rev. Condens. Matter Phys. **7**, 195 (2016).
[10] R. Schaffer, E. K.-H. Lee, B.-J. Yang, and Y. B. Kim, Rep. Prog. Phys. **79**, 094504 (2016).
[11] G. Cao and P. Schlottmann, Rep. Prog. Phys. **81**, 042502 (2018).
[12] A. Shitade, H. Katsura, J. Kunes, X.-L. Qi, S.-C. Zhang, and N. Nagaosa, Phys. Rev. Lett. **102**, 256403 (2009).
[13] G. Jackeli and G. Khaliullin, Phys. Rev. Lett. **102**, 017205 (2009).
[14] J. Chaloupka, G. Jackeli, and G. Khaliullin, Phys. Rev. Lett. **105**, 027204 (2010).
[15] C. H. Kim, H. S. Kim, H. Jeong, H. Jin, and J. Yu, Phys. Rev. Lett. **108**, 106401 (2012).
[16] H. S. Kim, C. H. Kim, H. Jeong, H. Jin, and J. Yu, Phys. Rev. B **87**, 165117 (2013).
[17] J. Reuther, R. Thomale, and S. Trebst, Phys. Rev. B **84**, 100406 (2011).
[18] X. Liu, T. Berlijn, W.-G. Yin, W. Ku, A. Tsvelik, Y.-J. Kim, H. Gretarsson, Y. Singh, P. Gegenwart, and J. P. Hill, Phys. Rev. B **83**, 220403 (2011).
[19] I. Kimchi and Y.-Z. You, Phys. Rev. B **84**, 180407 (2011).
[20] Y. Singh, S. Manni, J. Reuther, T. Berlijn, R. Thomale, W. Ku, S. Trebst, and P. Gegenwart, Phys. Rev. Lett. **108**, 127203 (2012).
[21] S. K. Choi, R. Coldea, A. N. Kolmogorov, T. Lancaster, I. I. Mazin, S. J. Blundell, P. G. Radaelli, Y. Singh, P. Gegenwart, K. R. Choi, S.-W. Cheong, P. J. Baker, C. Stock, and J. Taylor, Phys. Rev. Lett. **108**, 127204 (2012).
[22] C. C. Price and N. B. Perkins, Phys. Rev. Lett. **109**, 187201 (2012).
[23] F. Ye, S. X. Chi, H. B. Cao, B. C. Chakoumakos, J. A. Fernandez-Baca, R. Custelcean, T. F. Qi, O. B. Korneta, and G. Cao, Phys. Rev. B **85**, 180403 (2012).
[24] H. Gretarsson, J. P. Clancy, Y. Singh, P. Gegenwart, J. P. Hill, J. Kim, M. H. Upton, A. H. Said, D. Casa, T. Gog, and Y.-J. Kim, Phys. Rev. B **87**, 220407 (2013).
[25] G. Cao, T. F. Qi, L. Li, J. Terzic, V. S. Cao, S. J. Yuan, M. Tovar, G. Murthy, and R. K. Kaul, Phys. Rev. B **88**, 220414 (2013).
[26] J. Chaloupka, G. Jackeli, and G. Khaliullin, Phys. Rev. Lett. **110**, 097204 (2013).
[27] J. G. Rau, Eric Kin-Ho Lee, and H. Y. Kee, Phys. Rev. Lett. **112**, 077204 (2014).
[28] Y. Yamaji, Y. Nomura, M. Kurita, R. Arita, and M. Imada, Phys. Rev. Lett. **113**, 107201 (2014).
[29] Y. Yamaji, T. Suzuki, T. Yamada, S.-i. Suga, N. Kawashima, and M. Imada, Phys. Rev. B **93**, 174425 (2016).
[30] Y. Sizyuk, C. Price, P. Wölfle, and N. B. Perkins, Phys. Rev. B **90**, 155126 (2014).
[31] V. M. Katukuri, S. Nishimoto, V. Yushankhai, A. Stoyanova, H. Kandpal, and S. Choi, New J. Phys. **16**, 013056 (2014).
[32] K. Hu, F. Wang, and J. Feng, Phys. Rev. Lett. **115**, 167204 (2015).
[33] T. Suzuki, T. Yamada, Y. Yamaji, and S.-i. Suga, Phys. Rev. B **92**, 184411 (2015).
[34] S. H. Chun, J.-W. Kim, J. Kim, H. Zheng, C. C. Stoumpos, C. D. Malliakas, J. F. Mitchell, K. Mehlawat, Y. Singh, Y. Choi, T. Gog, A. Al-Zein, M. M. Sala, M. Krisch, J. Chaloupka, G. Jackeli, G. Khaliullin, and B. J. Kim, Nat. Phys. **11**, 462 (2015).
[35] A. Kitaev, Ann. Phys. (NY) **321**, 2 (2006).
[36] R. Comin, G. Levy, B. Ludbrook, Z.-H. Zhu, C. N. Veenstra, J. A. Rosen, Y. Singh, P. Gegenwart, D. Stricker, J. N. Hancock, D. van der Marel, I. S. Elfimov, and A. Damascelli, Phys. Rev. Lett. **109**, 266406 (2012).
[37] H. Gretarsson, J. P. Clancy, X. Liu, J. P. Hill, E. Bozin, Y. Singh, S. Manni, P. Gegenwart, J. Kim, A. H. Said, D. Casa, T. Gog, M. H. Upton, H.-S. Kim, J. Yu, V. M. Katukuri, L. Hozoi, J. van den Brink, and Y.-J. Kim, Phys. Rev. Lett. **110**, 076402 (2013).
[38] I. I. Mazin, H. O. Jeschke, K. Foyevtsova, R. Valentí, and D. I. Khomskii, Phys. Rev. Lett. **109**, 197201 (2012).
[39] K. Foyevtsova, H. O. Jeschke, I. I. Mazin, D. I. Khomskii, and R. Valentí, Phys. Rev. B **88**, 035107 (2013).
[40] C. H. Sohn, H.-S. Kim, T. F. Qi, D. W. Jeong, H. J. Park, H. K. Yoo, H. H. Kim, J.-Y. Kim, T. D. Kang, D.-Y. Cho, G. Cao, J. Yu, S. J. Moon, and T. W. Noh, Phys. Rev. B **88**, 085125 (2013).
[41] Y. Li, K. Foyevtsova, H. O. Jeschke, and R. Valentí, Phys. Rev. B **91**, 161101 (2015).
[42] B. H. Kim, T. Shirakawa, and S. Yunoki, Phys. Rev. Lett. **117**, 187201 (2016).
[43] Pressure-induced structural transition and reduction of the charge gap inferred from electrical transport were briefly mentioned in a conference abstract by Y. Singh, S. Layek, K. Mehlawat, E. Greenberg, G. K. Rozenberg, and M. P. Pasternak, http://meetings.aps.org/link/BAPS.2016.MAR.L33.11.

[44] X. Xi, C. Ma, Z. Liu, Z. Chen, W. Ku, H. Berger, C. Martin, D. B. Tanner, and G. L. Carr, Phys. Rev. Lett. **111**, 155701 (2013).

[45] D. Haskel, G. Fabbris, M. Zhernenkov, P. P. Kong, C. Q. Jin, G. Cao, and M. van Veenendaal, Phys. Rev. Lett. **109**, 027204 (2012).

[46] Drawings produced by VESTA. See K. Momma and F. Izumi, J. Appl. Crystallogr. **44**, 1272 (2011).

[47] See Supplemental Material at http://link.aps.org/supplemental/10.1103/PhysRevB.98.125117 for (i) x-ray diffraction data analysis, (ii) infrared phonon identification and fitting analysis, (iii) a more complete set of midinfrared absorbance, (iv) a phenomenological model for the interband transitions, (v) resistance data analysis, and (vi) methods for the first-principles calculations.

[48] V. Hermann, J. Ebad-Allah, F. Freund, I. M. Pietsch, A. Jesche, A. A. Tsirlin, J. Deisenhofer, M. Hanfland, P. Gegenwart, and C. A. Kuntscher, Phys. Rev. B **96**, 195137 (2017).

[49] K. Hu, Z. Zhou, Y.-W. Wei, C.-K. Li, and J. Feng, arXiv:1807.04413.

[50] N. F. Mott, *Conduction in Non-Crystalline Materials* (Oxford University Press, New York, 1993).

[51] $W \sim 4t$ is assumed in Ref. [38]. First-principles and tight-binding calculations for Na_2IrO_3 actually suggest $W < 2t$ for the low-lying bands (see, e.g., Ref [15]), which sets a lower bound for $\Delta t > 0.5\Delta E_g = 83$ meV.

[52] S. Bhattacharjee, S.-S. Lee, and Y. B. Kim, New J. Phys. **14**, 073015 (2012).

[53] X. Liu, V. M. Katukuri, L. Hozoi, W.-G. Yin, M. P. M. Dean, M. H. Upton, J. Kim, D. Casa, A. Said, T. Gog, T. F. Qi, G. Cao, A. M. Tsvelik, J. van den Brink, and J. P. Hill, Phys. Rev. Lett. **109**, 157401 (2012).

[54] P. S. Malavi, S. Karmakar, and S. M. Sharma, Phys. Rev. B **93**, 035139 (2016).

[55] Y. Zhao, W. Yang, N. Li, Y. Li, R. Tang, H. Li, H. Zhu, P. Zhu, and X. Wang, J. Phys. Chem. C **120**, 9436 (2016).

[56] S. J. Moon, H. Jin, W. S. Choi, J. S. Lee, S. S. A. Seo, J. Yu, G. Cao, T. W. Noh, and Y. S. Lee, Phys. Rev. B **80**, 195110 (2009).

[57] V. Hermann, M. Altmeyer, J. Ebad-Allah, F. Freund, A. Jesche, A. A. Tsirlin, M. Hanfland, P. Gegenwart, I. I. Mazin, D. I. Khomskii, R. Valentí, and C. A. Kuntscher, Phys. Rev. B **97**, 020104 (2018).

[58] J. P. Clancy, H. Gretarsson, J. A. Sears, Y. Singh, S. Desgreniers, K. Mehlawat, S. Layek, G. Kh. Rozenberg, Y. Ding, M. H. Upton, D. Casa, N. Chen, J. Im, Y. Lee, R. Yadav, L. Hozoi, D. Efremov, J. van den Brink, and Y.-J. Kim, npj Quantum Mater. **3**, 35 (2018).

[59] G. Bastien, G. Garbarino, R. Yadav, F. J. Martinez-Casado, R. Beltrán Rodríguez, Q. Stahl, M. Kusch, S. P. Limandri, R. Ray, P. Lampen-Kelley, D. G. Mandrus, S. E. Nagler, M. Roslova, A. Isaeva, T. Doert, L. Hozoi, A. U. B. Wolter, B. Büchner, J. Geck, and J. van den Brink, Phys. Rev. B **97**, 241108(R) (2018).

[60] T. Biesner, S. Biswas, W. Li, Y. Saito, A. Pustogow, M. Altmeyer, A. U. B. Wolter, B. Büchner, M. Roslova, T. Doert, S. M. Winter, R. Valentí, and M. Dressel, Phys. Rev. B **97**, 220401(R) (2018).